Environmental Fluid Mechanics
https://doi.org/10.1007/s10652-018-9644-2

ORIGINAL ARTICLE

Diffusion–dispersion numerical discretization for solute transport in 2D transient shallow flows

M. Morales-Hernández[1,2] · J. Murillo[1] · P. García-Navarro[1]

Received: 15 March 2018 / Accepted: 27 October 2018

Abstract
The 2D solute transport equation can be incorporated into the 2D shallow water equations in order to solve both flow and solute interactions in a coupled system of equations. In order to solve this system, an explicit finite volume scheme based on Roe's linearization is proposed. Moreover, it is feasible to decouple the solute transport equation from the hydrodynamic system in a conservative way. In this case, the advection part is solved in essence defining a numerical flux, allowing the use of higher order numerical schemes. However, the discretization of the diffusion–dispersion terms have to be carefully analysed. In particular, time-step restrictions linked to the nature of the solute equation itself as well as the numerical diffusion associated to the numerical scheme used are question of interest in this work. These improvements are tested in an analytical case as well as in a laboratory test case with a passive solute (fluorescein) released from a reservoir. Experimental measurements are compared against the numerical results obtained with the proposed model and a sensitivity analysis is carried out, confirming an agreement with the longitudinal coefficients and an underestimation of the transversal ones, respectively.

Keywords Solute transport · Diffusion–dispersion discretization · Shallow flows · Laboratory experiment · Mixing

1 Introduction

The controllability of contaminant releases in a shallow river has become an important issue in environmental impact analysis. Frequently, surface water systems are used for the dilution of wastes. In the past, simulation of this problems was based on steady one-dimensional analysis and design procedures aimed to minimize the impact on the environment. Recent developments in computational modelling of the fate and transport of the contaminants allow for accurate description of transient loading over complicated geometry and bathymetry of the riverine systems. As a results, it is possible to design contaminant

✉ M. Morales-Hernández
mmorales@unizar.es

[1] Fluid Mechanics, LIFTEC-EINA, CSIC-Universidad de Zaragoza, Zaragoza, Spain

[2] Soil and Water, EEAD-CSIC, Zaragoza, Spain

Published online: 01 November 2018

release strategies which can meet water quality criteria that are both temporally and spatially dependent.

In recent decades, the increasingly growing power of computers has directly enhanced the simulation of environmental problems. Fluvial hydrodynamics and transport can be modelled through numerical schemes capable of providing precise solutions even of a three-dimensional problem that contemplates the Navier–Stokes equations and the equation of transport. However, the applicability of such 3D models to practical problems is strongly restricted by the large amount of necessary physical information (geometry, turbulence parameters, friction parameters, turbulent diffusion coefficients) and the complex form of initial and boundary conditions. It is for this reason that, in the practice, much more simplified models of one and two spatial dimensions have become more widespread. For instance, the hydrodynamics of free surface flow is usually modelled with the Saint–Venant equations, while the transport is described by means of the depth averaged advection–diffusion–dispersion equation.

The modelling of the movement of a passive solute in natural streams or rivers includes (at least) two phenomena: the advection and the diffusion–dispersion effects. The convection–dispersion equation is well-justified from the physical point of view and there is abundant evidence that it reasonably describes the mixing process in many longitudinal flows (rivers and canals). It adapts well to a fast and efficient resolution methodology. However, either in its basic form or when combined with chemical and/or biological reaction terms, the resulting water quality model still depends on some parameters (dispersion coefficient, turbulent solubility coefficient …) that are not precisely determined. Therefore, it is mandatory to characterize these parameters relying on experimentation, both in laboratory and at field scale under various controlled conditions, for the evaluation of the distribution and evolution of variables that are relevant in the transport.

In a 2D depth-averaged model, these features are expressed by means of the well-known 2D advection–diffusion equation, which is usually linked to the 2D shallow water equations to solve the complex interactions that may occur in unsteady conditions. The resolution of these equations has been widely discussed in the literature. Traditionally, both transport and hydrodynamics equations were solved sequentially and independently [18, 26]. However, this approach may produce oscillations and does not guarantee the conservation property and the boundedness of the solution [13, 14]. In this work, a weakly coupled strategy is adopted based on [11, 17]. Based on the hydrodynamic information at each time step, it is feasible to build a suitable numerical flux for the solute transport equation that ensures conservation and positivity of the solution.

The choice of the adequate order of accuracy for the advection part of the solute transport equation has been deeply studied and the use of high-order schemes (at least second order of accuracy) is very popular in this context [22, 24]. They provide an accurate resolution of the solute concentration but the computational cost linked to their resolution and the fact that the velocity field is usually solved by means of a low-order scheme [12] makes them to be worthless in some situations. On the other hand, although first order schemes are a competitive solution in terms of computational burden, its numerical diffusion spread the solution, providing meaningless results.

The diffusion–dispersion terms in the solute transport equation need some adjustments that have to be carefully evaluated. First, their correct resolution is a challenge since they may dominate over the advection terms, deriving in dramatic restriction in the time step size and in a loss of hyperbolicity of the equations [14]. A multi-step explicit approach is proposed in this work to overcome this difficulty. Additionally, and linked to the resolution of the advection part, a modified first order scheme is proposed to solve the advection part,

using its own artificial diffusion to increase the accuracy until second order with a simple correction. These advances are tested using analytical test cases with exact solution under a steady flow configuration and with a laboratory experiment.

2 Governing equations and numerical scheme

2.1 Hydrodynamics and solute transport equations

The 2D shallow water equations, coupled to the depth averaged solute transport equation can be written in conservative form as follows:

$$\frac{\partial h}{\partial t} + \frac{\partial q_x}{\partial x} + \frac{\partial q_y}{\partial y} = 0 \tag{1}$$

$$\frac{\partial q_x}{\partial t} + \frac{\partial}{\partial x}\left(\frac{q_x^2}{h} + \frac{gh^2}{2}\right) + \frac{\partial}{\partial y}\left(\frac{q_x q_y}{h}\right) = gh(S_{ox} - S_{fx}) \tag{2}$$

$$\frac{\partial q_y}{\partial t} + \frac{\partial}{\partial x}\left(\frac{q_x q_y}{h}\right) + \frac{\partial}{\partial x}\left(\frac{q_y^2}{h} + \frac{gh^2}{2}\right) = gh(S_{oy} - S_{fy}) \tag{3}$$

$$\frac{\partial(h\phi)}{\partial t} + \frac{\partial(h\phi u)}{\partial x} + \frac{\partial(h\phi v)}{\partial y} = \vec{\nabla}(\mathbf{K}h\vec{\nabla}\phi) \tag{4}$$

where (1) represents the mass conservation of water, (2) and (3) refer to the momentum conservation in x and y directions respectively and (4) is the transport of a passive solute with a depth-average concentration of ϕ. Additionally, g is the gravity acceleration, q_x and q_y are the unit-discharges and $u = q_x/h$ and $v = q_y/h$ are the depth-averaged velocities in x and y directions respectively and h is the water depth. This system of partial differential equations can be written in a compact form:

$$\frac{\partial \mathbf{U}}{\partial t} + \frac{\partial \mathbf{F}(\mathbf{U})}{\partial x} + \frac{\partial \mathbf{G}(\mathbf{U})}{\partial y} = \mathbf{H}(\mathbf{U}) \tag{5}$$

where

$$\begin{aligned} &\mathbf{U} = \left(h, q_x, q_y, h\phi\right)^T \qquad \mathbf{F} = \left(q_x, \tfrac{q_x^2}{h} + \tfrac{1}{2}gh^2, \tfrac{q_x q_y}{h}, h\phi u\right)^T \\ &\mathbf{G} = \left(q_y, \tfrac{q_x q_y}{h}, \tfrac{q_y^2}{h} + \tfrac{1}{2}gh^2, h\phi v\right)^T \qquad \mathbf{H} = \left(0, gh(S_{0x} - S_{fx}), gh(S_{0y} - S_{fy}), \vec{\nabla}(\mathbf{K}h\vec{\nabla}\phi\right)^T \end{aligned} \tag{6}$$

being $\mathbf{U}$ the vector of conserved variables and $\mathbf{F}(\mathbf{U})$, $\mathbf{G}(\mathbf{U})$ the fluxes of these conserved variables. The source terms are included in $\mathbf{H}$, where S_{ox} and S_{oy} define the slopes in x and y directions being z the bottom level:

$$S_{ox} = -\frac{\partial z}{\partial x}, \quad S_{oy} = -\frac{\partial z}{\partial y}, \tag{7}$$

The friction losses S_f are modelled in terms of Manning's roughness coefficient n and are written for the x and y components as follows:

$$S_{fx} = \frac{n^2 u\sqrt{u^2+v^2}}{h^{4/3}}, \quad S_{fy} = \frac{n^2 v\sqrt{u^2+v^2}}{h^{4/3}} \tag{8}$$

Finally, $\mathbf{H}(\mathbf{U})$ also contains the diffusion–dispersion tensor $\mathbf{K}$. After some assumptions [20] of mainly turbulent flow it is feasible to neglect molecular diffusion and to express this tensor in the form of a diagonal matrix, only considering turbulent and gradient dispersion velocity terms:

$$\mathbf{K} = \begin{pmatrix} K_L & 0 \\ 0 & K_T \end{pmatrix} \tag{9}$$

being K_L and K_T the longitudinal and transversal coefficients respectively.

2.2 Numerical scheme

Following recent developments, the numerical resolution of the hydrodynamic part of the system (5) is performed by means of an explicit first order upwind scheme based on Roe's linearization [12, 15]. This ensures a robust and well balanced formulation. Although the details are omitted here since this is not the purpose of this work, the expression for the updating from time t^n to time t^{n+1} of the conserved hydrodynamic variables $\mathcal{U} = \left(h, q_x, q_y\right)$ at a single cell i with size A_i is included for completeness:

$$\mathcal{U}_i^{n+1} = \mathcal{U}_i^n - \frac{\Delta t}{A_i} \sum_{k=1}^{NE} \sum_{m}^{3} \left[(\tilde{\lambda}^- \tilde{\gamma}\, \tilde{\mathbf{e}})_k^m l_k \right]^n \tag{10}$$

In this expression, $\tilde{\lambda}$ and $\tilde{\mathbf{e}}$ are the eigenvalues and eigenvectors of the Jacobian matrix of the system (5), $\tilde{\gamma}$ contains the fluxes and source strengths, N_E indicates the number of edges in cell i ($N_E = 3$ for triangular cells) and l_k is the length of each neighbouring edge. It is worth noting the minus superscript denoting the upwind character of the proposed numerical scheme. Being an explicit scheme, the time step size Δt is limited by stability reasons in order to guarantee the CFL condition:

$$\Delta t = \mathrm{CFL}\, \frac{\min(\chi_i, \chi_j)}{\max_m |\tilde{\lambda}^m|} \qquad \chi_i = \frac{A_i}{\max_{k=1,N_E} l_k} \qquad \mathrm{CFL} \leq 1 \tag{11}$$

where χ_i is a characteristic distance defined by using the area of the cell as well as the length of the k neighbouring edges. This scheme has been proved to be robust, conservative, well-balanced and positivity preserving over irregular bed [15].

The numerical resolution of the solute transport equation under an explicit finite volume method is frequently performed by solving the depth-averaged concentration apart from the shallow water equations, that is, using a simpler decoupled algorithm. The scheme is easy: once the hydrodynamic equations have been solved in one time step, the corresponding substances or solutes are advected with these flow field quantities previously computed. However, careless numerical techniques lead to numerical troubles and do not preserve the conservation property [13], providing unbound non-physical results in certain cases.

In order to get a fully conservative method, the complete system including the hydrodynamic and the transport equations may be considered. Mathematically, the complete system conserves the hyperbolicity property, implying the existence of a 3×3 or 4×4 Jacobian matrix for the 1D or the 2D model respectively. On this basis we can apply the procedure described above, allowing a Roe's local linearization and expressing the contributions that arrive to the cell as a sum of waves. This scheme guarantees the conservation but it can lead to unbounded values in the final solute concentration in extreme cases. For this purpose, a strategy that avoids these situations by enforcing a conservative redistribution of the solute mass fluxes was proposed in [13].

It is feasible to decouple the solute transport equation from the hydrodynamic system in a conservative way as in [4], using a high resolution scheme that provides bounded solutions. However the time step is restricted to achieve the max–min property. A different technique is used in the present work for the solute transport. A thorough analysis of the augmented Riemann solver, considering all the set of possible approximate solutions in all kind of different flow situations for the volumetric concentration was presented in [17]. This analysis allowed to define in essence a single numerical flux $q^{\downarrow}$, directly related to the Roe's linearization, which is able to completely decouple the solute transport from the hydrodynamic system in a conservative way and to allow the use of a scheme with a different order of accuracy for the solute transport than for the hydrodynamics. For the sake of clarity, let us denote D_i the discretization of the diffusion–dispersion terms (which is explained afterwards). In this work, two numerical schemes are proposed:

2.2.1 First order scheme

In this case, the numerical flux is defined at each edge k separating cells i and j as follows:

$$q_k^{\downarrow} = q_i + \sum_{m=1}^{3} \left(\widetilde{\lambda}^{-} \, \widetilde{\gamma} \, \widetilde{\mathbf{e}}_1 \right)_k^m \tag{12}$$

where $q_i = (h\mathbf{u}\,\mathbf{n})_i$, $\mathbf{u} = (u, v)$ is the velocity vector and $\mathbf{n} = (n_x, n_y)$ is the normal vector from cell i to cell j. Accordingly, the numerical scheme for the solute transport equation is written as:

$$(h\phi)_i^{n+1} = (h\phi)_i^n - \frac{\Delta t}{A_i} \sum_{k=1}^{N_E} (q\phi)_k^{\downarrow} l_k + D_i \Delta t \tag{13}$$

where

$$\phi_k^{\downarrow} = \begin{cases} \phi_i & if \quad q_k^{\downarrow} > 0 \\ \phi_j & if \quad q_k^{\downarrow} < 0 \end{cases} \tag{14}$$

2.2.2 MUSCL-Hancock second order scheme

A two-step algorithm based on the MUSCL-Hancock scheme [25] is also explored in this work for triangular unstructured grids [8]. First, it is necessary to linearly reconstruct the

information at each cell i using limited gradient vectors $\overline{\mathbf{L}}_i$ according to the information provided by the neighbouring cells [8, 9]. The values at the edges (capital subscript) are then obtained according to the the position vectors $\mathbf{r}$ from the middle point M of the cell edge k to the centroid of the cell i:

$$\phi_{Ik} = \phi_i + r_{iM}\overline{\mathbf{L}}_i \tag{15}$$

Consequently, each interface k (sharing cells i and j) will contain two values ϕ_{Ik} and ϕ_{Jk} that represents a suitable reconstruction to the edge k from cells i and j respectively (see Fig. 1).

Once the variables are reconstructed, an intermediate step between time t^n and t^{n+1} is required to guarantee the second order accuracy in space and time:

$$\phi_{Ik}^{n+1/2} = u_{Ik}^n - \frac{\Delta t}{2A_i}\sum_{p=1}^{N_E}(\mathbf{un})_p(\delta\phi)_{Ip,i}^n\, l_p \tag{16}$$

where

$$(\delta\phi)_{Ip,i} = \phi_{Ip} - \phi_i \tag{17}$$

The second step is then computed, similar to that used for the first order scheme:

$$(h\phi)_i^{n+1} = (h\phi)_i^n - \frac{\Delta t}{A_i}\sum_{k=1}^{N_E}(q\phi)_k^{\downarrow} l_k + D_i\Delta t \tag{18}$$

where $q_k^{\downarrow}$ is defined as in (12) and

$$\phi_k^{\downarrow} = \begin{cases} \phi_{Ik}^{n+1/2} & if \quad q_k^{\downarrow} > 0 \\ \phi_{Jk}^{n+1/2} & if \quad q_k^{\downarrow} < 0 \end{cases} \tag{19}$$

3 Diffusion–dispersion discretization

The discretization of the diffusion–dispersion terms is addressed in this section. First, a way of avoiding a reduction in the time step size in the case of stiff diffusion-terms called Sub Step Explicit (SSE) is detailed. Then, two possible diffusion–dispersion models are

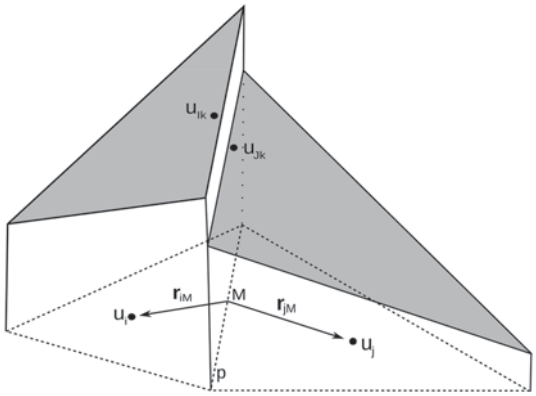

Fig. 1 Linear reconstruction for the MUSCL-Hancock approach

described which will be tested in a laboratory test case. Finally, a simple correction for the numerical diffusion in the first order scheme is explored.

3.1 Sub Step Explicit (SSE) resolution for the diffusion–dispersion terms

The resolution of the solute transport equation requires the computation of the term D_i in (13) or (18) (either for the first order or the second order scheme respectively). First of all, it is necessary to orient the diagonal matrix (9) in the direction of the flow at each point of the domain. Therefore, at each edge k, the following matrix $\mathbf{C}_k$ has to be estimated:

$$\mathbf{C}_k = \begin{pmatrix} D_{xx} & D_{xy} \\ D_{yx} & D_{yy} \end{pmatrix} = \begin{pmatrix} K_L \dfrac{\tilde{u}^2}{|\tilde{\mathbf{u}}|^2} + K_T \dfrac{\tilde{v}^2}{|\tilde{\mathbf{u}}|^2} & (K_L - K_T)\dfrac{\tilde{u}\tilde{v}}{|\tilde{\mathbf{u}}|^2} \\ (K_L - K_T)\dfrac{\tilde{u}\tilde{v}}{|\tilde{\mathbf{u}}|^2} & K_T \dfrac{\tilde{u}^2}{|\mathbf{u}|^2} + K_L \dfrac{\tilde{v}^2}{|\tilde{\mathbf{u}}|^2} \end{pmatrix} \tag{20}$$

Then, the discretized diffusion–dispersion term D_i can be approximated following Murillo and García-Navarro [16]:

$$D_i = \sum_{k=1}^{N_E} (\mathbf{Cnn})_k \frac{\tilde{h}_k \, l_k}{A_i \, d_{nk} \, h_i} \delta\phi_k = \sum_{k=1}^{N_E} B_k \delta\phi_k \tag{21}$$

where d_{nk} is the normal distance between cells i and j (sharing edge k). The term $\delta\phi_k$ can be estimated either implicitly or explicitly. Although the first approach provides an unconditionally stable scheme, the computation becomes expensive since iterative techniques are required. Therefore, an explicit approach $\delta\phi_k = (\phi_j - \phi_i)^n$ is adopted in this work. However, in order to ensure bounded values of the solution in (13) or (18), the following inequality must be satisfied

$$1 - \Delta t \sum_{k=1}^{N_E} B_k > 0 \tag{22}$$

leading to a new time step size Δt_d associated to the diffusion term:

$$\Delta t_d = \frac{1}{\sum_{k=1}^{N_E} B_k} \tag{23}$$

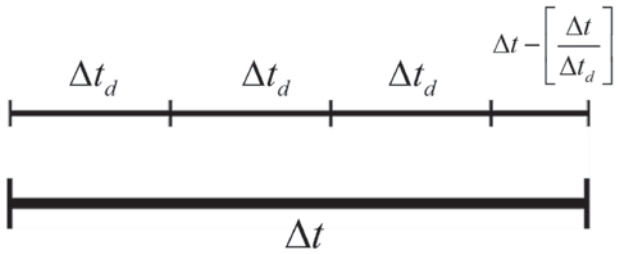

Fig. 2 Sketch of the SSE approach for the diffusion–dispersion discretization

Two possibilities arise in the case $\Delta t_d < \Delta t$: either reducing the global time step $\Delta t = \Delta t_d$ or splitting the whole time step Δt into several sub-time steps of size Δt_d, solving the diffusion subproblem each sub-step. The latter approach will be considered in this work. A sketch of the procedure is shown in Fig. 2, where the expression in brackets represents the integer part. It is worth highlighting that this approach is able to avoid the reduction in the time step size, achieving a better performance in terms of computational time.

3.2 Diffusion–dispersion model

Two models arise according to the definition of the friction velocity u^* and its components in 2D.

3.2.1 Standard anisotropic model

In this model, a matrix of the form (24) is used:

$$\mathbf{K} = \begin{pmatrix} K_L & 0 \\ 0 & K_T \end{pmatrix} = \begin{pmatrix} \epsilon_L h \mid u^* \mid & 0 \\ 0 & \epsilon_T h \mid u^* \mid \end{pmatrix} \tag{24}$$

The nature of the 2D numerical scheme leads to the definition of the friction velocity $\mid u^* \mid$ at each edge k (sharing cells i and j) as follows:

$$\mid u_k^* \mid = \sqrt{g\tilde{h}_k \cdot S_{f_k} \cdot} = n_k \sqrt{g \frac{\tilde{u}_k^2 + \tilde{v}_k^2}{\tilde{h}_k^{1/3}}} \tag{25}$$

where $n_k = \frac{1}{2}(n_i + n_j)$ is an averaged Manning's coefficient and the tilde variables are the averaged values coming from Roe's linearization:

$$\tilde{u}_k = \frac{\sqrt{h_i}\, u_i + \sqrt{h_j}\, u_j}{\sqrt{h_i} + \sqrt{h_j}}, \quad \tilde{v}_k = \frac{\sqrt{h_i}\, v_i + \sqrt{h_j}\, v_j}{\sqrt{h_i} + \sqrt{h_j}}, \quad \tilde{h}_k = \frac{h_i + h_j}{2} \tag{26}$$

Additionally, in expression (24) two coefficients ϵ_L and ϵ_T appear, called longitudinal and transversal dispersion coefficients respectively. In the literature, the most common values in rivers for these coefficients are [20]:

$$\epsilon_L = 5.93 \qquad \epsilon_T = 0.15 \tag{27}$$

Indeed, there exits a large amount of works in the literature devoted to this issue. Specially, the classical works of Taylor [23] and Fischer [5, 6] are considered as a reference. They were oriented to characterize the longitudinal and transversal mixing in straight and meandering channels and in natural streams, developing a background theory. Although this theory is still valid, some recent works with different experimental set-up's [1–3] adjust the original values and propose new methods to estimate them according to the shape, the curvature and the flow conditions.

3.2.2 Directional friction model

Contrary to the standard anisotropic model, this model only has to adjust only one coefficient $\overline{\epsilon}$ so that the diffusion–dispersion matrix for this model can be expressed as follows:

$$\mathbf{K} = \begin{pmatrix} K_L & 0 \\ 0 & K_T \end{pmatrix} = \begin{pmatrix} \overline{\epsilon} h u^* & 0 \\ 0 & \overline{\epsilon} h v^* \end{pmatrix} \tag{28}$$

However, the difference between longitudinal and transversal dispersion will be determined according to the computation of the friction velocities (at each edge k) for each direction [19]:

$$\begin{aligned} u_k^* &= n_k \sqrt{g \frac{\mid \tilde{u}_k \mid \sqrt{\tilde{u}_k^2 + \tilde{v}_k^2}}{\tilde{h}_k^{1/3}}} \\ v_k^* &= n_k \sqrt{g \frac{\mid \tilde{v}_k \mid \sqrt{\tilde{u}_k^2 + \tilde{v}_k^2}}{\tilde{h}_k^{1/3}}} \end{aligned} \tag{29}$$

where the tilde variables are defined as in (26).

3.3 Numerical diffusion correction

It is well known that the discretization and the numerical scheme chosen for the advection resolution of the solute transport equation introduce some artificial numerical diffusion. In particular, when doing an analysis for the transport equation with positive velocity $u > 0$ in 1D (only considering the advection and leaving aside the diffusion) for the first order upwind scheme of the diffusion–dispersion terms, the error made C^a can be expressed as follows:

$$C^a = \frac{1}{2} u(\Delta x - u \Delta t) \tag{30}$$

being Δt the time step size and Δx the mesh size. This error can be seen as an extra diffusion (numerical) added to the original equation. In the case of dealing with a real physical diffusion, it is important to compare both physical and numerical diffusions in order to avoid an overestimation that may affect the quality of the results. In the 2D framework, the artificial diffusion at each edge k, can be estimated as follows for the first order scheme:

$$C_k^a = \frac{1}{2} |\mathbf{un}| (d_{nk} - |\mathbf{un}| \Delta t) \tag{31}$$

Therefore the procedure is simple: if $C_k^a - (\mathbf{Cnn})_k > 0$ the numerical diffusion in (21) is set to 0, otherwise it is set to the difference between them $(\mathbf{Cnn})_k - C_k^a$. With this rule, the expression (21) for the discretization of the diffusion term D_i becomes:

$$D_i = \sum_{k=1}^{N_E} \mu_k \frac{\tilde{h}_k \, l_k}{A_i \, d_{nk} \, h_i} \delta \phi_k = \sum_{k=1}^{N_E} B_k \delta \phi_k \tag{32}$$

where $\mu_k = \max\left((\mathbf{Cnn})_k - C_k^a, 0\right)$. Note that $C_k^a = 0$ for the second order accurate scheme.

4 Analytical test case

This section is used to test the behaviour of the numerical schemes proposed in this work. The case consists of the evolution along t = 150 s of an sudden concentration release at point $P = (x_0, y0)$ in a [0,200 m] × [0,200 m] square domain. Assuming a constant velocity (1,1) all over the domain, the exact solution corresponds to a bidimensional Gaussian-shape function given by:

$$\phi(x,y,t) = \frac{M}{2\pi\sqrt{4t^2k}} exp\left[-\frac{(x-p_x)^2}{4tk/K_{yy}} - \frac{(y-p_y)^2}{4tk/K_{xx}} + \frac{(x-p_x)(y-p_y)}{2tk/K_{xy}}\right] \tag{33}$$

with

$$k = K_{xx}\cdot K_{yy} - K_{xy}^2 \quad ; \quad p_x = x_o + u\cdot t \quad ; \quad p_y = y_o + v\cdot t \tag{34}$$

In this computation, the following parameters are used:

$$\begin{aligned} &M = 100\cdot\pi \qquad t = 150s \qquad \mathbf{u} = (u,v) = (1,1) \qquad (x_o, y_o) = (15,15) \\ &p_x = 165 \qquad p_y = 165 \qquad K_{xx} = K_{yy} = 1.5 \qquad K_{xy} = K_{yx} = 0 \end{aligned} \tag{35}$$

Three different numerical schemes are tested: the first order scheme (13), the first order scheme (13) plus the numerical diffusion correction (32) and the MUSCL-Hancock second order scheme (18). A mesh convergence analysis is performed using four different triangular grids with around 25000, 75,000, 225,000 and 675,000 elements respectively (see Fig. 3).

Note that the diffusion has an isotropic character, that is, the longitudinal and transversal diffusion–dispersion values are the same: $K_L = K_T = 1.5$. The results obtained by each numerical scheme as well as the exact solution for each mesh are plotted in Fig. 4.

As expected, these qualitative results reveal that the first order scheme is very diffusive in comparison to the exact solution. However, the first order scheme with the numerical diffusion correction seems to behave as well as the second order scheme. In order to corroborate this hypothesis, a quantitative analysis is needed. In particular, the error norms L_1 and L_2 with respect to the exact solution are computed for each numerical scheme:

$$\| \, error \, \|_{L_1} = \frac{\sum_i^N \mid (\phi_e - \phi)_i \, A_i \mid}{A_T} \qquad \| \, error \, \|_{L_2} = \sqrt{\sum_i^N \frac{(\phi_e - \phi)_i^2 \, A_i}{A_T}} \tag{36}$$

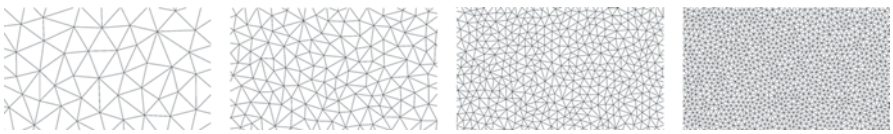

Fig. 3 Analytical test case: detail of the meshes. From left to right, mesh with 25000, 75000, 225000 and 675000 elements

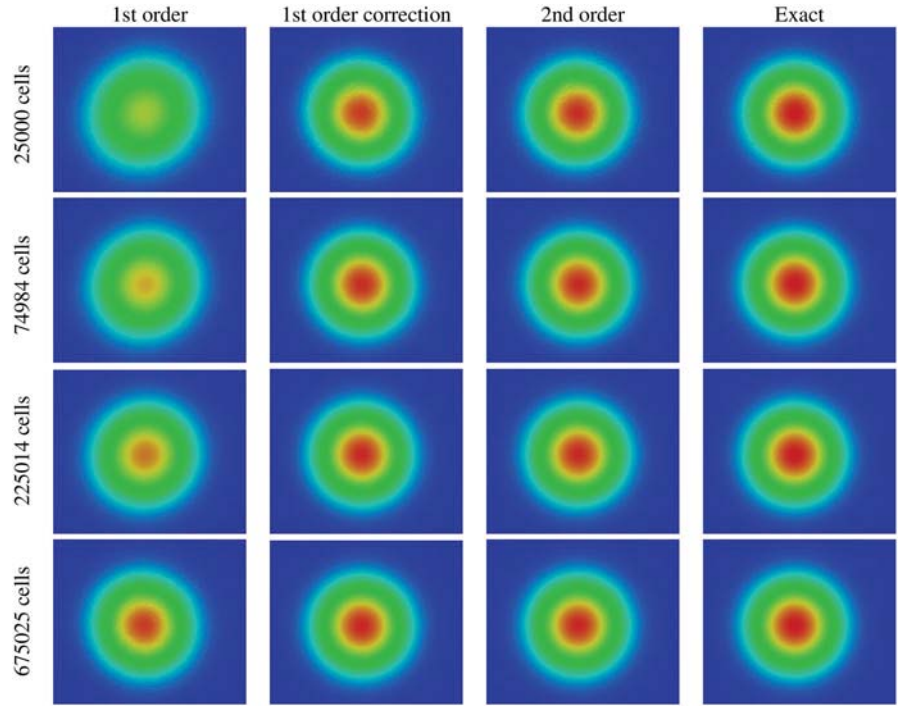

Fig. 4 Analytical test case: from left to right, result for the first order scheme, first order with correction, second order scheme and exact solution. From upper to lower, mesh size of 25,000, 74,984, 225,014 and 675,025 cells

Table 1 Analytical test case: L_1 and L_2 norms for first order scheme (1st order), first order scheme with correction (1st order C) and second order scheme (2nd order)

Ncells	L_1-error			L_2-error		
	1st order	1st order C	2nd order	1st order	1st order C	2nd order
25000	1.23e−3	2.52e−4	1.82e−4	3.62e−3	7.95e−4	5.67e−4
74984	1.23e−3	1.50e−5	1.40e−4	2.44e−3	4.70e−4	4.37e−4
225014	1.23e−3	1.05e−4	1.01e−4	1.59e−3	3.32e−4	3.21e−4
675025	1.23e−3	8.09e−5	8.13e−5	1.05e−3	2.55e−4	2.57e−4

being N the number of cells in the mesh, ϕ_{ei} the exact solution projected to each cell i of size A_i and A_T the total size of the mesh (constant). They are condensed in Table 1. As can be observed, the first order numerical scheme with correction achieves almost the same level of accuracy as the second order scheme, improving considerably the results obtained by the conventional first order scheme. In fact, the difference between them is negligible once the mesh is refined. Therefore, it can be concluded that, in problems where there exists a physical diffusion, the use of the first order scheme results highly desirable since it

possesses all the advantages of the conventional first order scheme and the level of accuracy of the second order scheme just using a simple correction.

5 Application to a laboratory test case

5.1 Setup description and experimental data

The laboratory facility used consists of a zero slope methacrylate rectangular channel 6m long and 0.24 m wide with an adjacent lateral reservoir controlled by a pneumatic gate and filled with water with fluorescein. Once a steady state of fresh water was enforced in the channel, the gate was suddenly opened (< 0.1 s) releasing the content of the reservoir that was washed by the channel flow. A measurement section was located at x = 3.07 m downstream the gate, where the temporal evolution of the concentration of fluorescein was registered. The sketch of the experiment is shown in Fig. 5. The channel inlet boundary condition was a steady discharge of $Q = 2.46\,\mathrm{m}^3/\mathrm{h}$ while a fixed Froude number of $Fr = 0.7437$ was imposed at the end of the channel. The reservoir was filled with 0.0085 m of water at rest with fluorescein.

The measurement sections was lighted up with an Ar+ laser, whose ultraviolet emission lines make the fluorescein to emit radiation with an intensity proportional to its concentration. A CCD camera with 30 frames per second was used. Therefore, the original data contain the temporal evolution of the fluorescein concentration in the measurement section. However, this information has to be averaged in the vertical direction in order to be compared with the depth-averaged proposed model. More details can be found in [7, 21]. The experiment data can be also downloaded in the following link: http://fiona.cps.unizar.es/~ghcuser/fluoresceineExperiment.txt.

5.2 Sensitivity analysis to the dispersion model

The computational mesh used to simulate this test case is made of 594269 unstructured triangles, where a local refinement has been applied in the zone influenced by the lateral reservoir. The initial condition is a steady state of $Q = 2.46\,\mathrm{m}^3/\mathrm{h}$ (previously computed) and the simulation time is 50 s. Although in the analytical test case the first order numerical

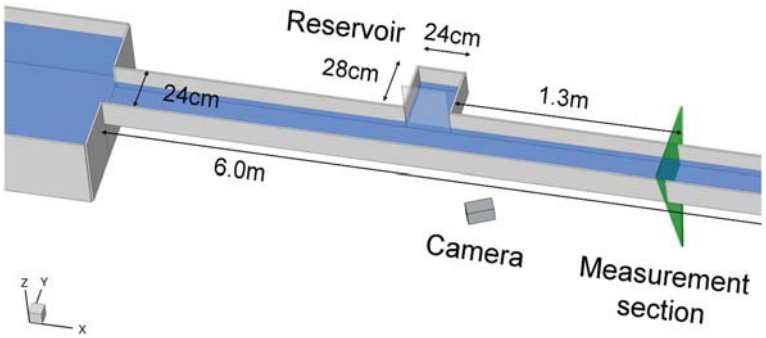

Fig. 5 Laboratory test case. Sketch of the experiment

scheme with correction has been proven as accurate as the second order scheme, a double simulation with the standard anisotropic model with $\epsilon_L = 5.93$ and $\epsilon_T = 0.15$ have been carried out in order to check this fact for this test case. The differences were negligible (in the order of 10^{-8}) hence the first order scheme with correction is chosen due to its simplicity and lower computational cost. With that scheme, each simulation run in GPU using CUDA [10] consumed around 1500s in a Nvidia GTX 780 card.

As stated in Sect. 3.2.1, the determination of longitudinal diffusion–dispersion coefficients it not straightforward hence a sensitivity analysis is conducted in order to estimate them in the mentioned laboratory test case. The final aim is to compare the best set of values (understood as those that achieve less error with respect to the experimental measurements) with the literature ones. As stated by Rutherford [20], it is advisable to choose a range of values and to carry out some sensitivity analysis given the large variations in published values of these coefficients.

The analysis consists of 49 simulations for the standard anisotropic model. Following the most recommended literature values ($\epsilon_L = 5.93$ and $\epsilon_T = 0.15$) the aim is to vary each coefficient one order of magnitude, that is, from half order of magnitude below to half order over that common value. Therefore the set of possible values for each coefficient is:

$$\epsilon_L = \{1.01, 2.65, 4.29, 5.93, 7.57, 9.2, 10.85\} \qquad \epsilon_T = \{0.03, 0.07, 0.11, 0.15, 0.19, 0.23, 0.27\} \tag{37}$$

Analogously, a sweep (11 simulations) for the coefficient $\overline{\epsilon}$ in the directional friction model is performed. It has been ranged from 1 to 11 (1 by one) due the lack of data for this parameter in the literature. In order to quantify the error made by each set of parameters, the L_1-norm of the error is chosen to perform the sensitivity analysis:

$$\| \, error \, \|_{L_1} = \frac{\sum_{t=0}^{t=50\,\mathrm{s}} | \, (\phi_M - \phi_S)_t}{N_T} \tag{38}$$

It is defined as the difference between measured (ϕ_M) and simulated ϕ_S results at the measurement section during all the experiment (N_T discrete times). Values of $\phi < 0.005$ are disregarded in both experimental and simulated data. The results are displayed in Tables 2 and 3 for the standard anisotropic model and the directional friction model respectively. They show the error made by each model and each corresponding coefficient. The bold value

Table 2 Laboratory test case. L_1-error for the standard anisotropic model

ϵ_L	ϵ_T						
	0.03	0.07	0.11	0.15	0.19	0.23	0.27
1.01	6.69e−3	6.37e−3	6.14e−3	5.97e−3	5.85e−3	5.77e−3	5.71e−3
2.65	5.10e−3	5.06e−3	5.04e−3	5.04e−3	5.06e−3	5.09e−3	5.12e−3
4.29	4.66e−3	4.70e−3	4.75e−3	4.81e−3	4.88e−3	4.95e−3	5.02e−3
5.93	**4.60e−3**	4.69e−3	4.79e−3	4.88e−3	4.98e−3	5.08e−3	5.17e−3
7.57	4.77e−3	4.88e−3	5.00e−3	5.12e−3	5.23e−3	5.34e−3	5.45e−3
9.2	5.06e−3	5.19e−3	5.32e−3	5.44e−3	5.56e−3	5.68e−3	5.79e−3
10.85	5.41e−3	5.54e−3	5.67e−3	5.80e−3	5.92e−3	6.03e−3	6.15e−3

Table 3 Laboratory test case. L_1-error for the directional friction model

$\overline{\epsilon}$	1.0	2.0	3.0	4.0	5.0	6.0
Error	5.76e−3	**4.89e−3**	4.95e−3	5.33e−3	5.85e−3	6.40e−3
$\overline{\epsilon}$	7.0	8.0	9.0	10.0	11.0	–
Error	6.93e−3	7.43e−3	7.91e−3	8.35e−3	8.76e−3	–

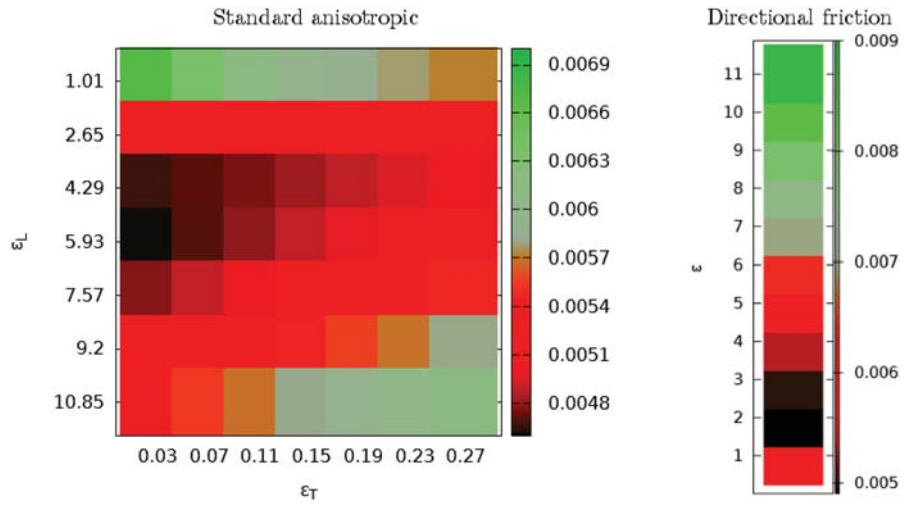

Fig. 6 Laboratory test case. Plots of L_1-error for standard anisotropic and directional friction models

corresponds to the best simulation understood as the configuration that achieves less error with respect to the measurement.

In order to plot the error in the form of a matrix and to analyze the sensitivity, Fig. 6 represents Tables 2 and 3, applying a colour scale to the error value.

For the standard anisotropic model, the minimum value of the error is reach for $\epsilon_L = 5.93$ and $\epsilon_T = 0.03$. Therefore, the value of minimum error is in concordance with the literature for the longitudinal dispersion, although the transversal dispersion is underestimated [20]. It may be caused by the fact that these values are usually characterized for mixing in rivers where the sinuosity and the curvature are different from this experiment. Regarding the results for the directional friction model, the minimum error is achieved for $\overline{\epsilon} = 2.0$. Although the lack of data for this parameter in the literature prevents a comparison as in the anisotropic model, the sensitivity of this parameter is greater than for the longitudinal and transversal coefficient. It is revealed in the difference between the maximum and minimum error, which is clearly greater than in the standard anisotropic model.

Finally, based on the results presented in Tables 2 and 3, a qualitative error is shown. The depth-averaged concentration is plotted in colour scale, while the time is represented in the abscissa axis and the width of the channel in the ordinate axis. Therefore, Fig. 7 displays the concentration profile for the experimental data (upper), the standard anisotropic

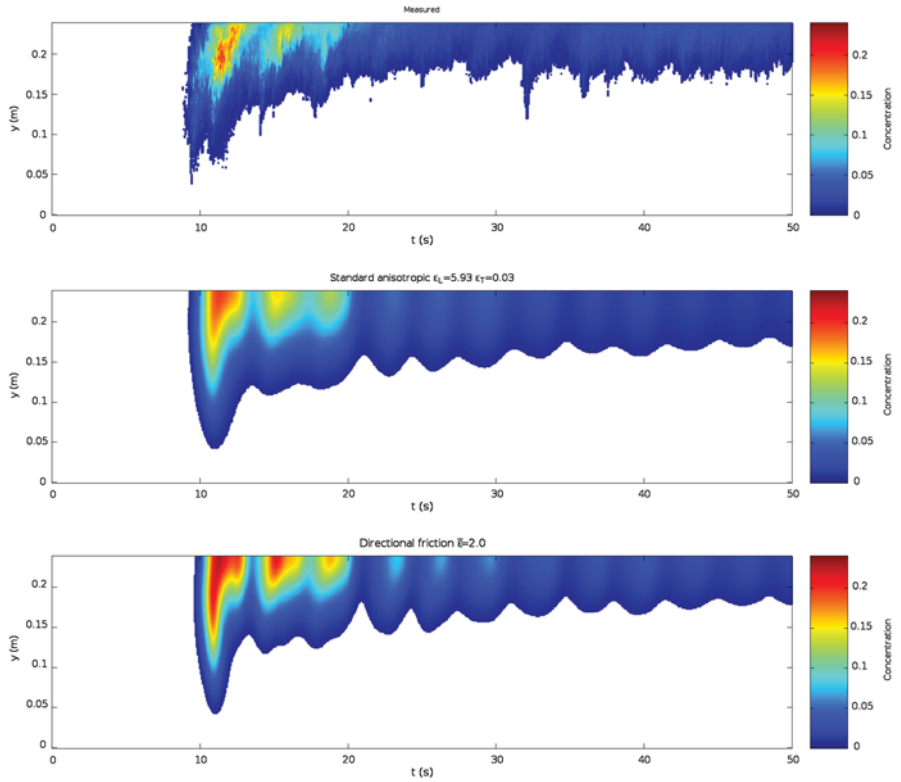

Fig. 7 Laboratory test case. Temporal evolution of depth-averaged concentration at the measurement section. Experimental data (upper), standard anisotropic model with $\epsilon_L = 5.93$ and $\epsilon_T = 0.03$ (middle) and directional friction model with $\overline{\epsilon} = 2.0$ (lower)

with $\epsilon_L = 5.93$ and $\epsilon_T = 0.03$ (middle) and the directional friction with $\overline{\epsilon} = 2.0$. They correspond to the simulations with minimum error for each model. Although the standard anisotropic model reproduce better the experimental measurements, both models are able to reproduce satisfactorily the time of arrival of the maximum concentration peak (around $t = 11$ s). Additionally, the shape of the fluorescein concentration shows a good agreement with respect to the experimental data.

In this qualitative analysis, the worse results in terms of L_1-error for each model (according to Tables 2 and 3) are also included. For each model, the underestimation and overestimation of the coefficients is displayed in Fig. 8. In particular, for the standard anisotropic model the underestimation and overestimation is achieved when using $\epsilon_L = 1.01; \epsilon_T = 0.03$ and $\epsilon_L = 10.85; \epsilon_T = 0.27$ respectively. For the directional friction model, these results correspond to $\overline{\epsilon} = 1.0$ and $\overline{\epsilon} = 11.0$.

Regarding these results, the main conclusion that can be deduced is the high influence of the coefficients in the behaviour of the concentration. It is specially noticeable the shape of the fluorescein for greater coefficient, where the profile is completely smeared out.

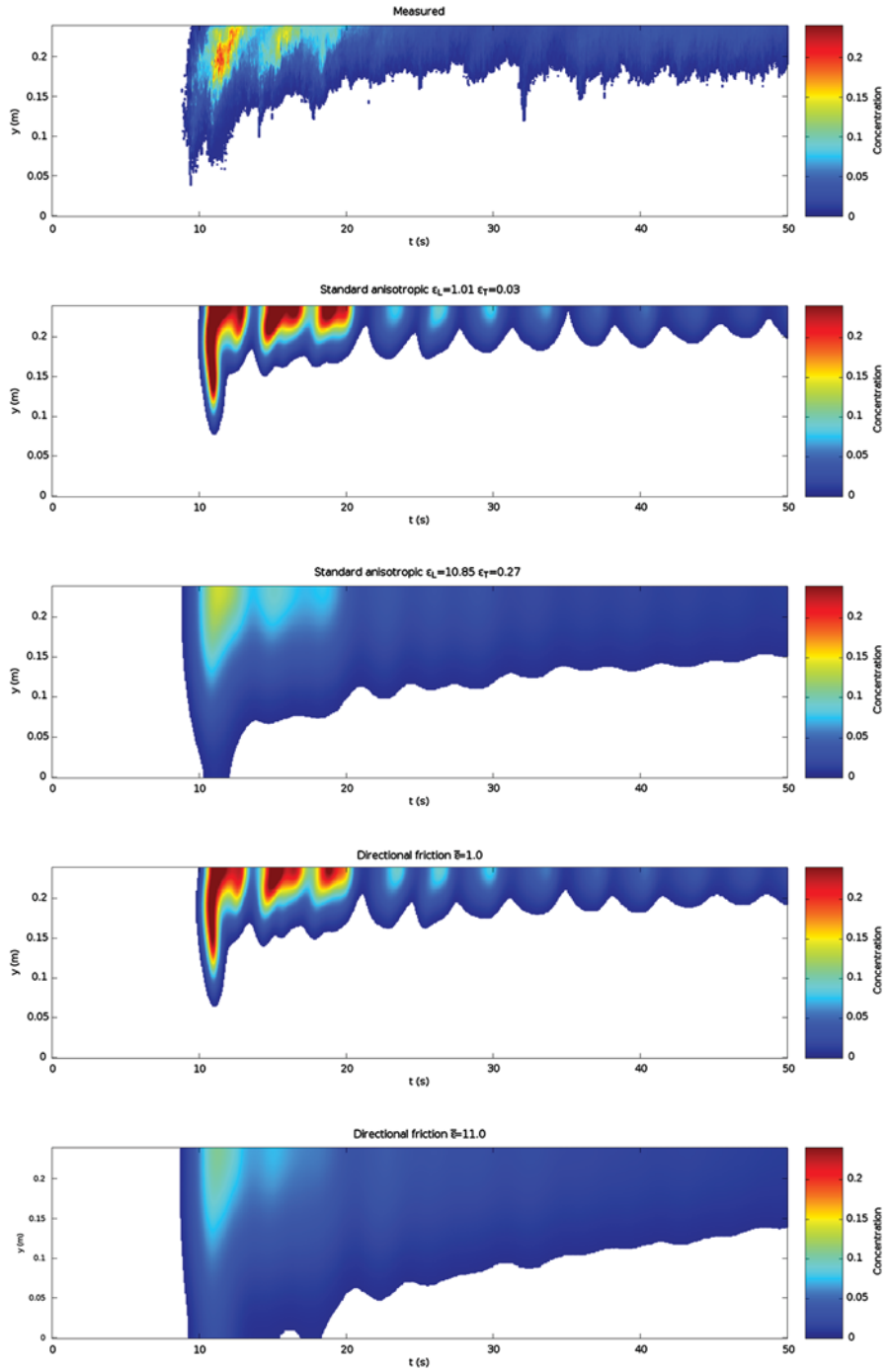

Fig. 8 Laboratory test case. Temporal evolution of depth-averaged concentration at the measurement section. From upper to lower, experimental data, standard anisotropic model with $\epsilon_L = 1.01; \epsilon_T = 0.03$, standard anisotropic model with $\epsilon_L = 10.85; \epsilon_T = 0.27$, directional friction model with $\overline{\epsilon} = 1.0$ and directional friction model with $\overline{\epsilon} = 11.0$

6 Conclusions and perspectives

The advection–diffusion–dispersion equation is well justified from the physical point of view and there is abundant evidence that it reasonably describes the depth averaged mixing process in many flows (rivers and channels). Some improvements in connection to the numerical resolution of the solute transport equation with diffusion–dispersion terms have been proposed in this work. First, a conservative decoupled formulation of the solute transport equation from the hydrodynamic systems is explained, based on the construction of the numerical flux through the edges. This strategy allows the use of a different numerical scheme for the resolution of the solute transport equation of that used for the hydrodynamic system.

Regarding the discretization of the diffusion–dispersion terms, a Sub Step Explicit technique is adopted in this work, which is able to avoid a reduction in the time step size when the diffusion terms dominate over the convective terms. A simple and cheap improvement for the first order upwind scheme is described, consisting in estimating the numerical diffusion that the method artificially introduces and to compare with the physical one. This strategy has been proven to be as accurate as the second order scheme (MUSCL-Hancock reconstruction) for the analytical test case proposed.

Finally two diffusion–dispersion models are detailed and analyzed for a laboratory test case. The standard anisotropic model seems to represent better the experimental data than the directional friction model in the laboratory experiment. A sensitivity analysis has been carried out concluding that, although the longitudinal coefficient matches the literature values, the transversal coefficient is somehow underestimated.

The proposed advances are directly connected with the efficiency and accuracy of the models that are able to predict quantitative variables such as water depth, flow velocities or chemical species concentration. The utilization of fast and reliable predictive tools will represent a breakthrough in this field in the next few years. For instance, this methodology can be used as a basis to evaluate contaminant release episodes in rivers, where some parameters are not known with sufficient precision. However, it is necessary to keep in mind that experimentation, both laboratory and field, is also essential for the evaluation of the distribution and evolution of the relevant variables in transport under various controlled conditions.

Acknowledgements This work was partially funded by the MINECO/FEDER under research project CGL2015-66114-R and by Diputación General de Aragón, DGA, through Fondo Europeo de Desarrollo Regional, FEDER.

References

1. Baek KO, Seo IW (2010) Routing procedures for observed dispersion coefficients in two-dimensional river mixing. Adv Water Resour 33:1551–1559
2. Baek KO, Seo IW (2016) On the methods for determining the transverse dispersion coefficient in river mixing. Adv Water Resour 90:1–9
3. Boxall JB, Guymer I (2003) Analysis and prediction of transverse mixing coefficients in natural channels. J Hydraul Eng 129:129–139
4. Casulli V, Zanolli P (2005) High resolution methods for multidimensional advection–diffusion problems in free-surface hydrodynamics. Ocean Model 10(1–2):137–151
5. Fischer HB (1967) The mechanics of dispersion in natural streams. J Hydraul Div Am Soc Civ Eng 93(6):187–215
6. Fischer HB (1969) The effects of bends on dispersion in streams. Water Resour Res 5(2):496–506

7. García JA, Latorre B, López-Barrera D, Ambroj S (2008) Experimental measurements of solute transport and flow velocity in a laboratory channel. In: 8th international conference on hydroscience & engineering ICHE 2008
8. Hou J, Liang Q, Simons F, Hinkelmann R (2013) A 2D well-balanced shallow flow model for unstructured grids with novel slope source term treatment. Adv Water Resour 52:107–131
9. Hubbard ME (1999) Multidimensional slope limiters for MUSCL-type finite volume schemes on unstructured grids. J Comput Phys 155:54–74
10. Lacasta A, Morales-Hernández M, Murillo J, García-Navarro P (2014) An optimized GPU implementation of a 2D free surface simulation model on unstructured meshes. Adv Eng Softw 78:1–15
11. Latorre B, García-Navarro P, Murillo J, Burguete J (2011) Accurate and efficient simulation of transport in multidimensional flow. Int J Numer Methods Fluids 65:405–431
12. Morales-Hernández M, Petaccia G, Brufau P, García-Navarro P (2016) Conservative 1D–2D coupled numerical strategies applied to river flooding: the Tiber (Rome). Appl Math Model 40(3):2087–2105
13. Murillo J, García-Navarro P, Burguete J (2008) Analysis of a second-order upwind method for the simulation of solute transport in 2D shallow water flow. Int J Numer Methods Fluids 56(6):661–686
14. Murillo J, Burguete J, Brufau P, García-Navarro P (2005) Coupling between shallow water and solute flow equations: analysis and management of source terms in 2D. Int J Numer Methods Fluids 49:267–299
15. Murillo J, García-Navarro P (2010) Weak solutions for partial differential equations with source terms: application to the shallow water equations. J Comput Phys 229:4327–4368
16. Murillo J, García-Navarro P (2011) Improved Riemann solvers for complex transport in two-dimensional unsteady shallow flow. J Comput Phys 230(19):7202–7239
17. Murillo J, Latorre B, García-Navarro P (2012) A Riemann solver for unsteady computation of 2D shallow flows with variable density. J Comput Phys 231(14):4775–4807
18. Playán E, García-Navarro P, Zapata N (2000) Solute transport modelling in overland flow applied to fertigation. J Irrig Drain Eng 126(1):33–40
19. Rodi W (1988) Turbulence models and their application in hydraulics a state of the art review. Special IAHR Publication, Beijing
20. Rutherford JC (1994) River mixing. Wiley, Chichester
21. Burillo G Sánchez, Murillo J, García-Navarro P, Monreal P, Latorre B (2011) Numerical simulation of advection–diffusion of a passive solute in unsteady water flow. In: 3rd conference turbulent mixing and beyond
22. Shi J, Zhang Y-T, Shu C-W (2003) Resolution of high order WENO schemes for complicated flow structures. J Comput Phys 186:690–696
23. Taylor GI (1954) The dispersion of matter in turbulent flow through a pipe. Proc R Soc Lond Ser A 233:446–468
24. Titarev VA, Toro EF (2002) ADER: arbitrary high order Godunov approach. J Sci Comput 17:609–618
25. van Leer B (1979) Towards the ultimate conservative difference scheme. V. A second-order sequel to Godunov's method. J Comput Phys 32:101–136
26. Yan M, Kahawita R (2006) Modeling spatial and temporal variation of a pollutant in water environment using the cubic spline scheme. J Hydrodyn Ser B 18(6):688–697